Clays and Clay Minerals, Vol. 66, No. 1, 28–42, 2018.

HYDROTHERMAL EXPERIMENTS REVEAL THE INFLUENCE OF ORGANIC MATTER ON SMECTITE ILLITIZATION

JINGONG CAI[1,*], JIAZONG DU[1], ZEWEN CHEN[1], TIANZHU LEI[2], AND XIAOJUN ZHU[1]

[1]State Key Laboratory of Marine Geology, Tongji University, 200092, Shanghai, China
[2]Lanzhou Institute of Geology, Chinese Academy of Sciences, 730000, Lanzhou, China

Abstract—Smectite illitization is an important diagenetic phenomenon of mudstones, but only rarely has the influence of organic matter (OM) on this process been examined. In the present study, hydrothermal experiments were conducted with smectite (M1, total organic carbon (TOC) <0.3%) and a smectite and N,N-dimethylhexadecylamine (16DMA) complex (M2, TOC >1%). X-ray diffraction (XRD), infrared, X-ray fluorescence (XRF), and organic carbon analyses were employed to characterize the mineralogy and OM of the samples and the effect of OM on smectite illitization. The XRD patterns showed changes in clay mineral parameters with increased temperature. These changes varied in both M1 and M2 and indicated a difference in the degree of smectite illitization. Moreover, the OM in M2 was mainly adsorbed in smectite interlayers, the OM was largely desorbed/decomposed at temperatures above 350ºC, and the OM was the main reason for differences in the degree of smectite illitization between M1 and M2. Bulk mineral composition, elemental content, and infrared absorption band intensities were changed with increased temperature (especially above 350ºC). This indicated the formation of new minerals (*e.g.*, ankerite). Overall, OM entered the interlayer space of smectite in M2 and delayed the exchange of K^+ by interlayer cations, and thus, suppressed the transformation of smectite to illite and resulted in differences in smectite illitization of M1 and M2. In particular, the formation of CO_2 after the decomposition of OM at temperatures above 300ºC led to the formation of ankerite in M2. This demonstrated the effect of organic-inorganic interactions on smectite illitization and mineral formation. The disparities in smectite illitization between M1 and M2, therefore, were linked to differences in the mineral formation mechanisms of a water-rock system (M1) and a water-rock-OM system (M2) in natural environments. The insights obtained in the present study should be of high importance in understanding organic-mineral interactions, hydrocarbon generation, and the carbon cycle.

Key Words—Hydrothermal Experiments, Mineral Formation Mechanism, OM Occurrence, Smectite, Smectite Illitization, Smectite-organic Complex.

INTRODUCTION

Smectite illitization is the process of smectite-to-illite transformation (Altaner and Ylagan, 1997), which is an important diagenetic process of mudstones in most sedimentary basins around the world (Burst, 1969; Pearson and Small, 1988; Velde and Vasseur, 1992). Mudstones in sedimentary basins are composed of minerals (*e.g.*, detrital minerals, clay minerals, and carbonates), pore water, and organic matter (OM) (Tissot and Welte, 1984; Tyson, 1993; Li and David, 2005; Pacton *et al.*, 2011). Two types of mudstone are distinguished based on the abundance of OM. One type of mudstone has relatively high OM contents, such as carbonaceous mudstones, oil shale, and source rocks; the OM content is little to none in the other type of mudstones, such as mottled and red mudstones. This raises questions on the role of OM in smectite illitization of mudstones.

Over 90% of the OM in mudstones is combined with clay-size minerals (Cai, 2004; Leithold *et al.*, 2005; Dickens *et al.*, 2006), which can be present in diverse forms, *e.g.*, in the pore space, on the external surfaces of clay crystals, or in clay mineral interlayers (Kennedy *et al.*, 2002; Cai *et al.*, 2007). Specifically, minerals may adsorb OM in different ways (Lasaga and Luttge, 2001; Kothawala *et al.*, 2012). Smectite that strongly expands can adsorb large amounts of OM in the interlayers and to external surfaces (Yariv and Cross, 2002) *via* a 'water bridge' or the exchangeable cations, such as Ca^{2+}, Mg^{2+}, Fe^{3+}, and Al^{3+} (Theng, 1979; Pusino *et al.*, 1993). Further studies have found that an organo-clay complex, which is prepared by the adsorption of a single-chain alkyl ammonium salt to Na-smectite, is very stable (He *et al.*, 2006; Parbhakar *et al.*, 2007) and has an interlayer spacing that can reach 4.5 nm (Armstrong and Chesters, 1964). Illite is a non-expandable clay mineral and only adsorbs OM on external surfaces (Theng, 1979). Such different types of adsorbed OM might have important effects on smectite illitization. In recent years, the influence of OM on mineral formation has been increasingly examined (Egli *et al.*, 2001; Arnarson and

* E-mail address of corresponding author:
jgcai@tongji.edu.cn
DOI: 10.1346/CCMN.2017.064084

This paper was originally presented during the 3rd Asian Clay Conference, November 2016, in Guangzhou, China

Keil, 2007; Naderizadeh *et al.*, 2010; Pérez *et al.*, 2011; Hanke *et al.*, 2014; Li *et al.*, 2016) and more attention has been given to the effects of OM on cation activity (Berthelin, 2010; Greenwood *et al.*, 2013). As such, mineral transformations in the presence of OM is also of great significance.

Both smectite and illite are 2:1 phyllosilicates in which each individual clay layer is composed of two tetrahedral sheets and one octahedral sheet (Grim, 1953; Eberl, 1978; Cuadros and Altaner, 1998). The interlayers contain interlayer water and hydrated cations (*e.g.*, Ca^{2+}, Mg^{2+}, and Na^{+}) in smectite (Wang, 1998; He *et al.*, 1999; Liu *et al.*, 2005), and K^{+} in illite (Xu and Harsh, 1992). The above properties result in differences in interlayer spacing, expandability, cation exchange capacity (CEC), specific surface area, and other properties. Various mechanisms for the smectite to illite transformation have been proposed (Pollard, 1971; Ahn and Peacor, 1986; Altaner and Ylagan, 1997; Baronnet, 1997; Putnis, 2002; Cuadros, 2012) and the broadly accepted mechanisms are solid-state transformation (Hower *et al.*, 1976; Bethke and Altaner, 1986; Drits *et al.*, 1997; Cuadros and Altaner, 1998; Olives *et al.*, 2000) and dissolution-recrystallization (Boles and Franks, 1979; Nadeau *et al.*, 1985; Eberl and Srodon, 1988; Whitney and Velde, 1993; Mosser-Ruck *et al.*, 1999; Mosser-Ruck *et al.*, 2001; Lanson *et al.*, 2009). The solid-state transformation mechanism was first introduced by Hower *et al.*, (1976) and states that as Si^{4+} in the tetrahedral sheets and Al^{3+} in the octahedral sheets are substituted by Al^{3+} and Mg^{2+}, respectively, the interlayer water is then expelled and K^{+} is sequestered in the interlayers to ultimately form illite. The dissolution-recrystallization mechanism emphasizes the dissolution of smectite structural layers and the recrystallization of illite. Specifically, 1 mole of smectite is converted into 1 mole of illite (Nadeau *et al.*, 1985; Inoue *et al.*, 1987; Inoue *et al.*, 1990; Środoń *et al.*, 1992; Altaner and Ylagan, 1997). In a large number of hydrothermal investigations, researchers have emphasized the importance of parameters that affect smectite illitization, such as the water/rock ratio (Howard and Roy, 1985; Whitney, 1990; Mayer, 1994), the cation concentrations (Roberson and Lahann, 1981; Huang *et al.*, 1993; Mosser-Ruck *et al.*, 2001; Cai *et al.*, 2007), the porosity/permeability (Ramseyer and Boles, 1986), and temperature/time (Perry and Hower, 1970; Cuadros and Linares, 1996; Putnis, 2002). The influence of OM on smectite illitization, however, has scarcely been investigated. The purpose of the present study was, therefore, to fill this gap by investigating further the role of OM in the illitization of smectite by submitting smectite and a N,N-dimethylhexadecylamine (16DMA)-smectite complex to hydrothermal treatments at different temperatures in a closed system, followed by measurement of the mineralogy and OM characteristics of the products obtained.

MATERIALS AND METHODS

Sample preparation

The smectite used for this study was from a smectite quarry in Chifeng, Inner Mongolia, China. Prior to the experiments, the <2 μm clay fraction of the raw smectite was separated in accordance with Stokes' Law for purification and dried at room temperature. The N,N-dimethylhexadecylamine (16DMA) ($C_{18}H_{39}N$; molecular weight = 269.5) was purchased from Sun Chemical Technology (Shanghai, China) Co., Ltd.

The <2 μm smectite was first Na-saturated and was then mixed with 16DMA to make a 16DMA-smectite complex. For the Na-smectite (M1) sample, the <2 μm smectite was suspended in 5 mol/L NaCl solution for 48 h, washed with deionized water until the filtrate was Cl^{-} free as indicated by testing with an $AgNO_3$ solution, and the suspension was then collected and dried. For the 16DMA-smectite complex (M2), a certain amount of M1 was dispersed in deionized water and mixed for 24 h with a quantity of 16DMA solution equal to 1.0 × CEC of the smectite using a magnetic stirrer. The suspension was then allowed to stand until it flocculated, the supernatant was decanted and discarded, and the solid residue was collected and dried. Both the M1 and M2 preparations were dried in an oven at 60ºC and ground to <200-mesh for subsequent use.

Hydrothermal experiments

In a typical experiment, stoichiometric amounts of M1 and M2 were weighed and placed into a FYX1 autoclave (Dalian Tongchan High-Pressure Reactor Manufacturing Company, Dalian, China) and 1 mol/L KCl solution (pH=8−9) was added to create a 3:1 water/rock mass ratio. The mixture was then covered and sealed to form a closed system.

The hydrothermal treatments were at 100, 200, 250, 300, 350, 400, 450, and 550 ±2ºC for 72 h with a temperature increase rate of 1ºC/min. At temperatures below 350ºC, the pressure was equal to the saturated vapor pressure of water, which is 0.10, 1.55, 3.98, 8.59, and 16.53 MPa, respectively, at temperatures of 100, 200, 250, 300, and 350ºC. At temperatures of 350 to 550ºC, the pressures were kept at a constant 16.53 MPa. Room temperature in this paper will, henceforth, be assumed to be 25ºC. Equivalent sample masses were used in all hydrothermal experiments to minimize systematic errors.

After the hydrothermal experiments were completed, the sample residues in the autoclave were recovered using centrifugation, washed with deionized water, and dried in an oven at 60ºC. Excess 16DMA was extracted from the dried samples using dichloromethane for more than 72 h in a Soxhlet apparatus, and the solids were then collected for subsequent measurement. The total organic carbon (TOC) contents in the original M1 and M2 samples were 0.27 and 16.02, respectively.

https://doi.org/10.1346/CCMN.2017.064084 Published online by Cambridge University Press

Measurement methods

X-ray diffraction analysis. The X-ray diffraction (XRD) analyses were performed using a X'PERT-PRO-MPD diffractometer (PANalytical, Amelo, The Netherlands) using a CuK X-ray tube at 40 mA and 40 kV with a curved graphite monochromator. The CuKα radiation wavelength was 1.540596 Å. The scattering slit was 1º and the receiving slit was 0.3 mm. Each oriented slide was scanned from 3 to 30º2θ at 2º2θ/min using a step width of 0.02º2θ. The randomly oriented powder mounts were scanned from 3 to 40º2θ at 2º2θ/min using a step width of 0.02º2θ.

Clay composition analyses were conducted using the oriented slides and multiple treatments: air-dried (Na-saturated), ethylene glycol saturation, and heating (550ºC). The 100−550ºC thermal treatments in the XRD analyses were used to examine variations in the smectite or illite-smectite (I-S) interlayer spacings. Previous XRD analyses of heated soil samples (Theng *et al.*, 1986) and argillaceous source rocks (Cai *et al.*, 2007) suggest that water adsorbed in the interlayer space of clay minerals is readily removed by heating to 250ºC, whereas the interlayer OM is more stable. The relevant basal spacings of organo-clay complexes were greater than 10 Å until the temperature of 550ºC was reached. As such, the 250 and 550ºC heat treatments are accepted as two significant points in the thermal treatment and XRD analysis which can be used to determine the stability of interlayer OM (Nemecz, 1981). For this reason, three different treatments were used on the oriented slides in the present study to detect changes in smectite or I-S interlayer spacings: air drying (Na-saturated), heating to 250ºC, and heating to 550ºC.

The clay minerals were identified based on the position of the (001) series of basal reflections in the air-dried, ethylene glycol-saturated, and heated (550ºC) XRD sample patterns. Partial mineral quantification was performed by calculating the integrated peak areas of the mineral phases and by multiplying the peak areas by in-house calibrated and/or published weighting factors. The integrated peak area of the 7 Å (chlorite 002/kaolinite 001) peak in the ethylene glycol-treated sample XRD pattern was used to quantify the amounts of chlorite and kaolinite. The relative proportions of these two minerals were based on the peak heights of kaolinite 002 (3.58 Å) and chlorite 004 (3.52 Å) on the glycolated patterns. The quantities of smectite, I-S, and illite were based on the integrated areas of the 10-Å peak for the 550ºC heated XRD patterns. The quantities of smectite were based on the integrated area of the ethylene glycol treatment 17-Å peak, whereas illite quantities were based on the integrated areas of the 10-Å peak. The quantity of I-S was based on the remaining fraction, *i.e.*, I-S = (100 − (%kaolinite + %chlorite + %illite + %smectite)). The chlorite/kaolinite, smectite, and illite weighting factors were 2/3, 1/4, and 1, respectively. Replicate analyses of a few selected samples gave a relative precision of ±2%.

Bulk mineralogy analyses were performed on the randomly oriented powder mounts. The quantity of each mineral was based on the integrated peak areas of each mineral phase.

The stacking mode (R, Reichweite ordering parameter), percent illite in the I-S (%I in I-S), and the average number of layers (N_{ave}) in the I-S stacking sequence were determined using the method of Moore and Reynolds (1997) and the computer software, NEWMOD 2.0 (Reynolds, 1985). The precision of the %I in I-S quantification was determined to be ±5%.

X-ray fluorescence analysis. The major element concentrations were analyzed using an AXIOSmax instrument (PANalytical, Amelo, The Netherlands) using the fusion method for sample preparation. The measurements were based on calibrations that followed the National Standard method (GBT 14506.28-2010). Replicate analyses of five selected samples gave a relative precision of ±0.1%.

Fourier Transform infrared (FTIR) spectroscopy. Infrared (IR) spectra in the middle infrared region (MIR, 4000−400 cm^{-1}) were obtained using a Nicolet 6700 spectrometer (ThermoFisher Scientific, Waltham, Massachusetts, USA) equipped with a diffuse reflectance accessory using the sum of 128 scans at a resolution of 4 cm^{-1} and a mirror velocity of 0.6329 cm/s. To obtain the IR spectra, a dueterated triglycine sulfate (DTGS) detector and a KBr beam splitter were used. The <2 μm fractions were manually ground in an agate mortar for 15 min. Subsequently, the powders were heated at 105ºC for 24 h and then stored in a desiccator with solid silica gel at room temperature. Approximately 200 mg of the thermally treated powder from each sample was prepared for the analyses. Spectroscopy-grade KBr was used for the background spectrum. Smoothing and normalization of the spectra were performed using the OMNIC 8 software package (Nicolet Instruments Corporation).

NIR spectroscopy. IR spectra in the near infrared region (NIR, 1250-2500 nm) were obtained using a Perkin-Elmer Lambda 6 spectrophotometer (PerkinElmer, Waltham, Massachusetts, USA) with a diffuse reflectance attachment. Sample preparation and analysis followed the procedures described by Balsam and Deaton (1991) and Pentrák *et al.*, (2012). The <2 μm fractions were made into a slurry on a glass microslide with distilled water, smoothed, slowly dried at low temperature (<40ºC), heated at 105ºC for 24 h, and then cooled to room temperature for 2 h in a desiccator with solid silica gel. Spectral analyses were performed using OMNIC 8 software. The second-order derivatives of the NIR bands were analyzed using Norris gap derivative filters using default OMNIC parameters.

https://doi.org/10.1346/CCMN.2017.064084 Published online by Cambridge University Press

Total organic carbon (TOC) analysis. An Elementar Vario EL Cube analyzer (Elementar, Langenselbold, Hesse, Germany) was employed to measure organic carbon. Samples were placed in crucibles and dried at low temperature (<40ºC). Approximately 10 mg of each sample was wrapped with Al foil and tested on the organic element analyzer. Measurement errors were found to be less than 0.2%.

RESULTS

XRD analysis

The XRD patterns indicated that the bulk mineralogy of all samples of M1 and M2 were dominated by clay minerals with a low content of detrital minerals (quartz, K-feldspar, and plagioclase) and other minerals (halite, ankerite). With an increased treatment temperature, the clay content decreased, while the content of detrital minerals and other minerals increased. In particular, ankerite was detected in samples with treatment temperatures >300ºC (Table 1, Figure 1).

The main clay minerals were smectite/I-S and illite. The M1 smectite/I-S content was 72.9% on average and lower than M2, which averaged 77.9%. The average illite content was higher in M1 (26.3%) than in M2 (19.6%) (Table 1; Figures 2a, 2b). Kaolinite and chlorite were detected in samples treated at temperatures between 100ºC and 350ºC, but the contents were less than 5% (Table 1; Figures 2c, 2d). The evolution of clay minerals with temperature showed two stages (Figure 2). When the treatment temperature was below 350ºC, the smectite/I-S content in M1 (80.3%) was lower than in M2 (90.3%) (Figure 2b),

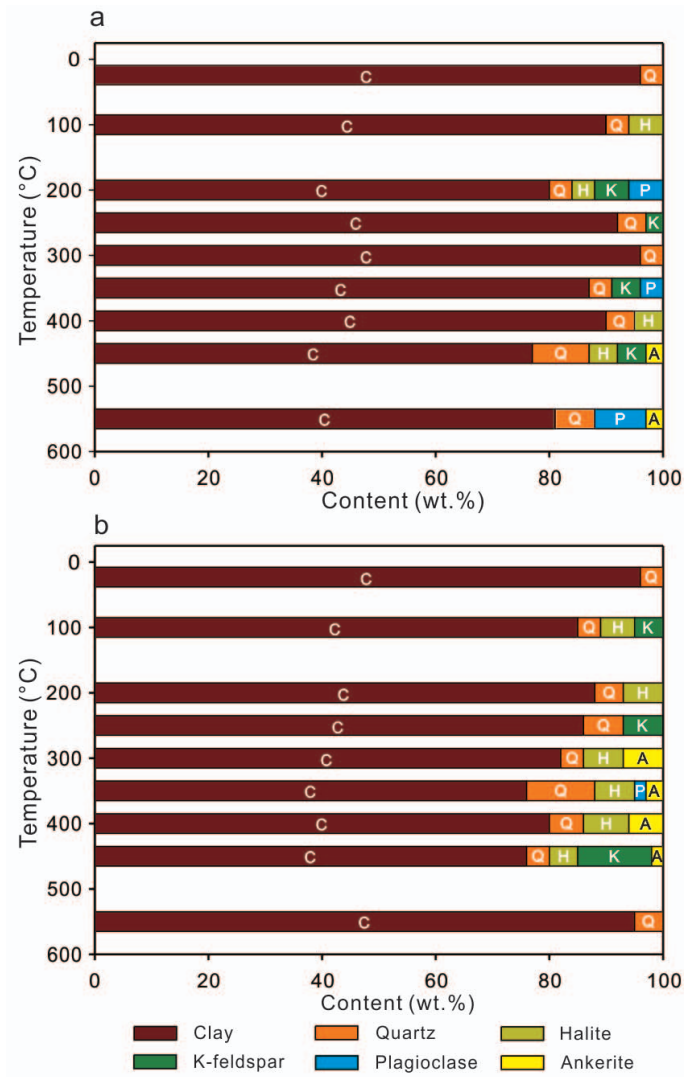

Figure 1. Clay content and bulk mineralogy of M1 (a) and M2 (b) at different temperatures. Abbreviations for the minerals are within the bars (C: clay mineral, Q: quartz, H: halite, K: K-feldspar, P: plagioclase, A: ankerite).

https://doi.org/10.1346/CCMN.2017.064084 Published online by Cambridge University Press

Table 1. Data for the bulk mineralogy, clay mineralogy, TOC, and elemental content of the M1 and M2 samples.

Sample	*T* (ºC)	Mineral content (wt.%)						Clay content (wt.%)				I-S parameter				TOC	Elements content (wt.%)										
		Clay	Quartz	hlite	K-feld-spar	Plagio-clase	anker ite	Kao-linite	Chlor-ite	Illite	Smec-tite	%I in I-S	R	N	N_{ave}	(wt.%)	SiO_2	A_2O_3	K_2O	Fe_2O_3	MgO	CaO	Na_2O	MnO	P_2O_5	TiO_2	SO_3
M1	25	96	4	0	0	0	0	0	0	0	100	2	R0	0	0	0.27	62.47	16.67	0.13	4.99	4.86	0.49	3.31	0.03	0.02	0.32	0.017
M1	100	90	4	6	0	0	0	0	0	13	87	46	R0	0	0	0.60	60.74	16.20	5.95	5.28	4.61	0.18	0.51	0.04	0.02	0.31	0.020
M1	200	80	4	4	6	6	0	2	3	10	85	51	R0	0	0	0.23	57.36	15.36	7.94	4.95	4.32	0.24	1.21	0.03	0.01	0.29	0.017
M1	250	92	5	0	3	0	0	1	1	26	72	56	R0	1–2	1.5	0.23	60.22	16.15	6.17	4.91	4.67	0.19	0.57	0.03	0.02	0.30	0.017
M1	300	96	4	0	0	0	0	0	0	32	68	61	R0	2–3	2.5	0.26	61.07	16.37	6.03	5.28	4.63	0.14	0.38	0.04	0.02	0.31	0.020
M1	350	87	4	0	5	4	0	0	0	30	70	66	R0.5	2–4	3	0.24	–	–	–	–	–	–	–	–	–	–	–
M1	400	90	5	5	0	0	0	0	0	37	63	78	R0.5	3–4	3.5	0.26	57.49	15.47	8.21	6.71	4.26	0.13	0.61	0.03	0.02	0.30	0.020
M1	450	77	10	5	5	0	3	0	0	35	65	84	R1	4–6	5	0.33	56.79	15.69	8.84	7.63	4.49	0.11	0.52	0.04	0.02	0.30	0.025
M1	550	81	7	0	0	9	3	0	0	54	46	89	R1.5	6–7	6.5	0.27	60.12	16.14	4.52	8.14	4.70	0.41	2.31	0.07	0.02	0.31	0.018
M2	25	96	4	0	0	0	0	0	0	0	100	2	R0	0	0	16.02	49.60	13.36	0.09	4.30	3.88	0.39	2.73	0.02	0.01	0.25	0.009
M2	100	85	4	6	5	0	0	3	4	0	93	40	R0	0	0	5.17	56.53	15.08	5.28	4.66	4.36	0.30	0.41	0.03	0.02	0.29	0.007
M2	200	88	5	7	0	0	0	4	4	0	92	43	R0	0	0	3.01	58.18	15.59	5.60	4.77	4.54	0.34	0.36	0.03	0.02	0.29	0.015
M2	250	86	7	0	7	0	0	0	0	0	100	42	R0	1–2	1.5	5.21	56.71	14.99	6.15	4.60	4.30	0.11	0.06	0.03	0.03	0.29	0.007
M2	300	82	4	7	0	0	7	2	2	13	83	50	R0	1–3	2	3.86	56.86	15.22	6.17	4.84	4.39	0.27	0.44	0.03	0.02	0.28	0.015
M2	350	76	12	7	0	2	3	3	3	20	74	78	R0	2–4	3	1.30	59.82	15.22	7.29	4.89	4.37	0.34	0.45	0.03	0.02	0.29	0.016
M2	400	80	6	8	0	0	6	0	0	48	54	81	R0.5	2–4	3	1.02	58.38	15.69	7.51	6.09	4.58	0.15	0.51	0.04	0.02	0.29	0.019
M2	450	76	4	5	13	0	2	0	0	38	62	80	R0.5	2–5	3.5	2.37	57.05	15.35	5.98	7.51	4.48	0.25	1.52	0.05	0.02	0.29	0.010
M2	550	95	5	0	0	0	0	0	0	57	43	84	R1	1–7	4	4.85	57.48	15.47	2.87	5.46	4.53	0.40	2.09	0.04	0.02	0.29	0.008

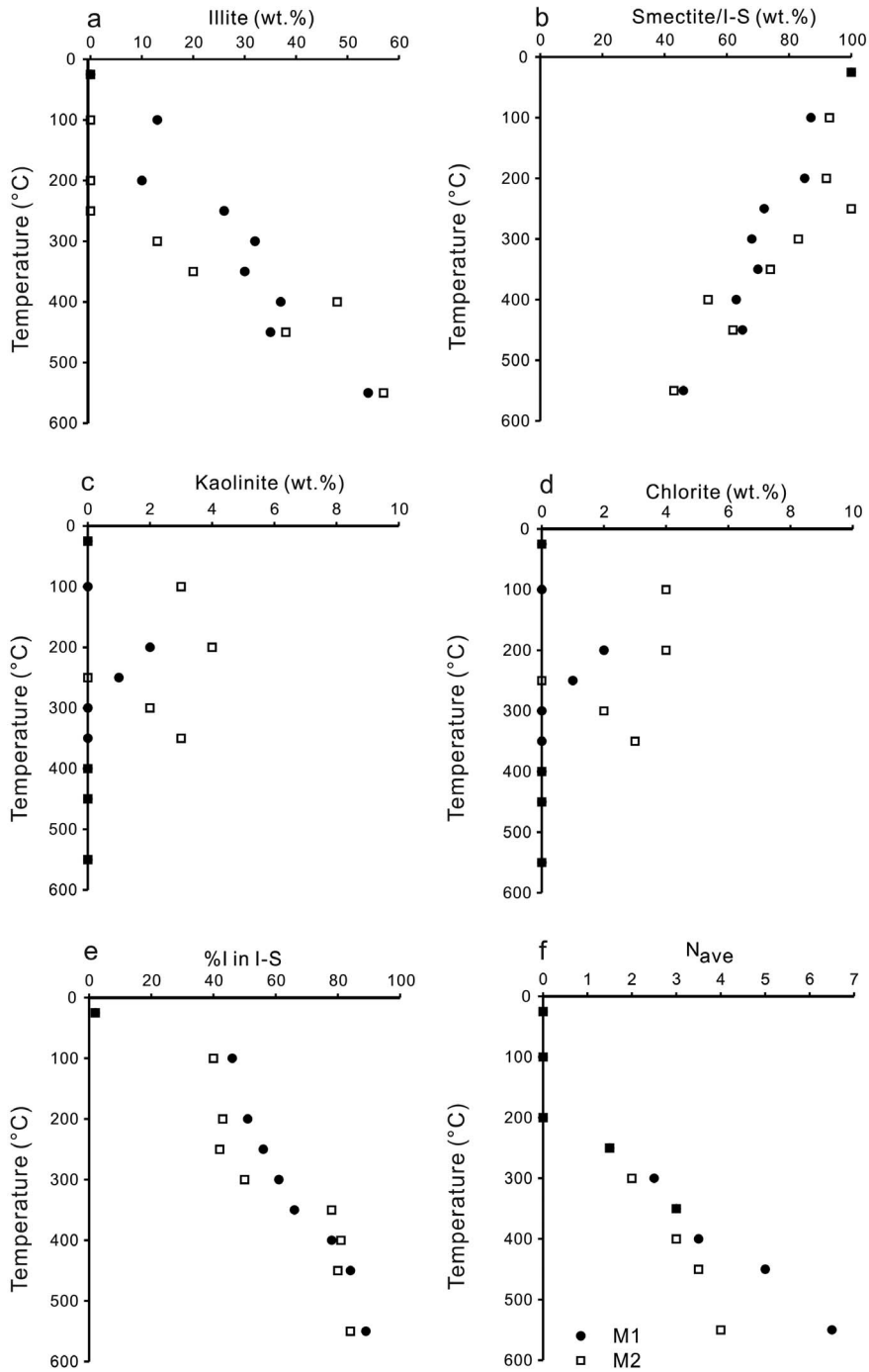

Figure 2. Scatter diagrams of the clay mineral contents in M1 and M2: (a–d) %illite, %smectite, %kaolinite, and %chlorite; (e) %illite in I-S; and (f) average number of layers in I-S (N_{ave}) in M1 and M2.

while the illite content in M1 (18.5%) was higher than in M2 (5.5%) (Figure 2a). When the temperature was above 350ºC, the rates of M1 smectite/I-S and illite content changes were similar to the rates at below 350ºC (Figures 2a, 2b). For M2, the smectite/I-S and illite content change rate increased at temperatures above 350ºC, the illite content reached 47.7%, and the smectite/I-S content decreased to 53% (Figures 2a, 2b). In addition, the kaolinite and chlorite contents in M2 were greater than in M1 at each treatment temperature (Figures 2c, 2d).

The %I in I-S of M1 was positively correlated with temperature (R^2>0.9; Figure 2e). With a temperature

https://doi.org/10.1346/CCMN.2017.064084 Published online by Cambridge University Press

increase from 100 to 550ºC, the %I in I-S of M1 steadily increased from 46 to 89% (Table 1; Figure 2e). The relationship between %I in I-S and temperature for M2 showed two stages (Figure 2e): %I in I-S slowly increased from 40 to 50% with a treatment temperature increase from 100 to 300ºC, sharply increased to 78% at 350ºC, and slowly increased to 84% when the temperature increased from 350 to 550ºC, which showed a jumpy trend in evolution.

At treatment temperatures of 250 to 550ºC, N_{ave} increased from 1.5 to 6.5 in M1 and from 1.5 to 4 in M2 (Table 1; Figure 2f). This indicated a higher overall rate of increase in N_{ave} with temperature in M1 than in M2. Differences in the N_{ave} increase rates for M1 and M2 were particularly large between 300 and 350ºC.

With an increased temperature, the I-S stacking mode increased from R0 to R1.5 in M1 and from R0 to R1 in M2 (Table 1; Figure 3). The stacking mode changes were less at lower temperatures with R0.5 at 350ºC for both M1 and M2. At 550ºC, the stacking mode in M1 (R1.5) was greater than in M2 (R1), which indicates that the changes in M2 were greater than in M1 at higher temperatures.

The XRD patterns of heated samples at each treatment temperature showed that the d_{001} values for M1 under the three treatments were almost the same, except for the $M1_{25ºC}$ treatment (Figure 4a). In the XRD patterns of the M2 samples heated at <350ºC, the d_{001} value of the air-dried sample was nearly the same as the 250ºC treatment, but was very different than the 550ºC treatment. For treatment temperatures above 350ºC, the differences between the d_{001} values for the three treatments were smaller and almost disappeared at 550ºC (Figure 4b). These results indicate that the OM in M2 was different in samples treated at temperatures <350ºC and >350ºC.

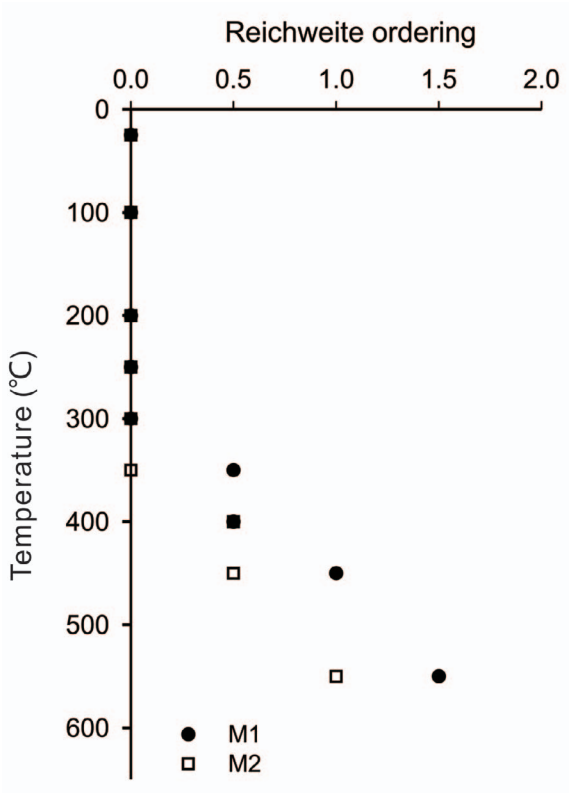

Figure 3. Reichweite ordering to indicate the effect of temperature on the I-S stacking mode in the M1 and M2 smectite samples.

Elemental analysis

The XRF analyses of the M1 and M2 samples measured Si, Al, Ca, and Mg contents that did not change noticeably with increased temperature. Obvious changes in the K, Na, and Fe contents, however, were observed with increased temperature. The K contents increased in M1 samples heated at 100 to 450ºC and in M2 samples heated at 100 to 400ºC, but the K contents decreased in samples heated at >400ºC. In contrast, the Na contents of samples heated at >400ºC generally increased. The Fe contents of $M1_{25ºC}$ and $M2_{25ºC}$ were 4.99% and 4.30%, respectively. Heating generally increased the relative Fe contents in M1 samples heated from 100 to 300ºC and M2 samples heated from 100 to 350ºC (Figure 5).

Total organic carbon (TOC) contents

The TOC contents of M1 samples were low with average values of less than 0.30% (Table 1; Figure 6). The TOC contents of M2 samples, however, were much higher with an average value of 4.76% and a maximum value of 16.02% for $M2_{25ºC}$. The M1 sample TOC contents were relatively stable with increased heating temperature and only fluctuated between 0.23 and 0.60%. The M2 sample TOC contents were >3.01% in samples heated at <300ºC and <2.37% in M2 samples heated at >300ºC, except for the $M2_{550ºC}$ sample.

Infrared analysis

FTIR (4000–400 cm^{-1}) analysis. In the spectroscopic analyses of M1, several specific absorption bands were observed: The band at 3625 cm^{-1} was attributed to the stretching vibration of OH in smectite; the band at 1630 cm^{-1} was due to the bending vibration of OH from adsorbed water; both the 1100 and 990 cm^{-1} bands were attributed to antisymmetric stretching vibrations of Si-O from the tetrahedral sheet; and the 919 and 752 cm^{-1} bands were attributed to the bending vibration of Al-OH from the octahedral sheet. Intensities of the bands at 3625, 919, and 752 cm^{-1} changed slightly with increased temperature, while the OH bending vibration intensity at 1630 cm^{-1} gradually decreased after heating at 350 to 550ºC. The intensities of bands at 1100 and 990 cm^{-1} progressively decreased with increased temperature and almost disappeared at temperatures >450ºC (Figure 7a).

https://doi.org/10.1346/CCMN.2017.064084 Published online by Cambridge University Press

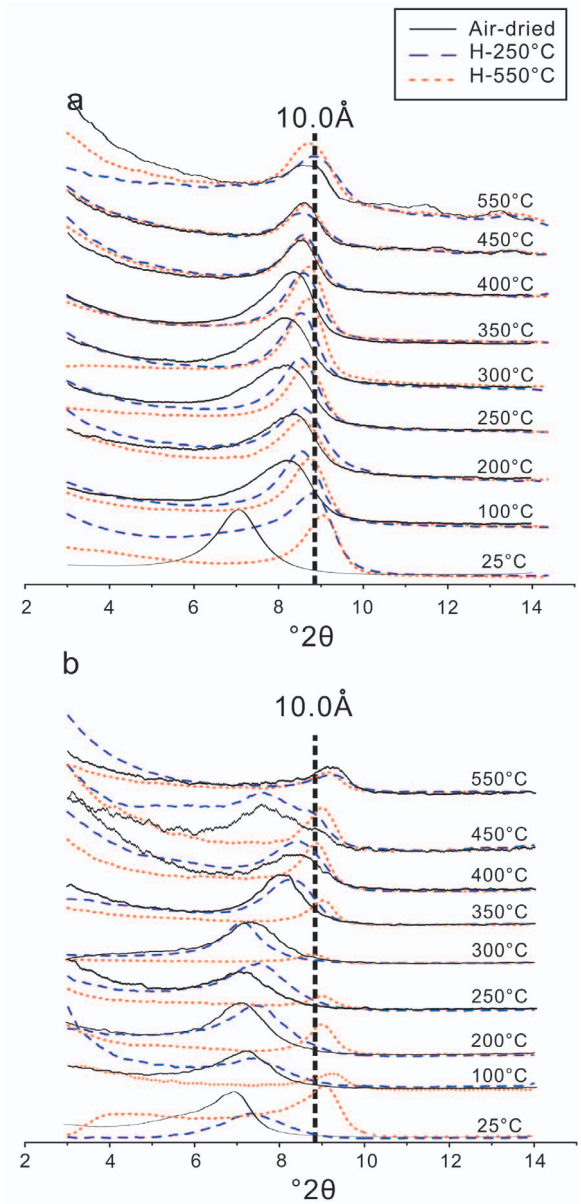

Figure 4. X-ray diffraction patterns for (a) M1 and (b) M2 samples that were air-dried (solid line), heated to 250ºC (dashed line), or heated to 550ºC (dotted line).

The specific FTIR absorption bands observed in M2 included bands also observed in M1 and the bands evolved similarly with increased temperatures. Moreover, the M2 FTIR spectra also had antisymmetric and symmetric stretching modes of aliphatic CH_2 at 2926 and 2852 cm^{-1}, respectively, and the CH bending vibration at 1471 cm^{-1} (Figure 7b). The band intensities of the three vibrations dramatically decreased when the treatment temperatures were >350ºC and disappeared at 550ºC. This suggests that the form of the OM adsorbed to the minerals changed and that the OM was lost at 550ºC.

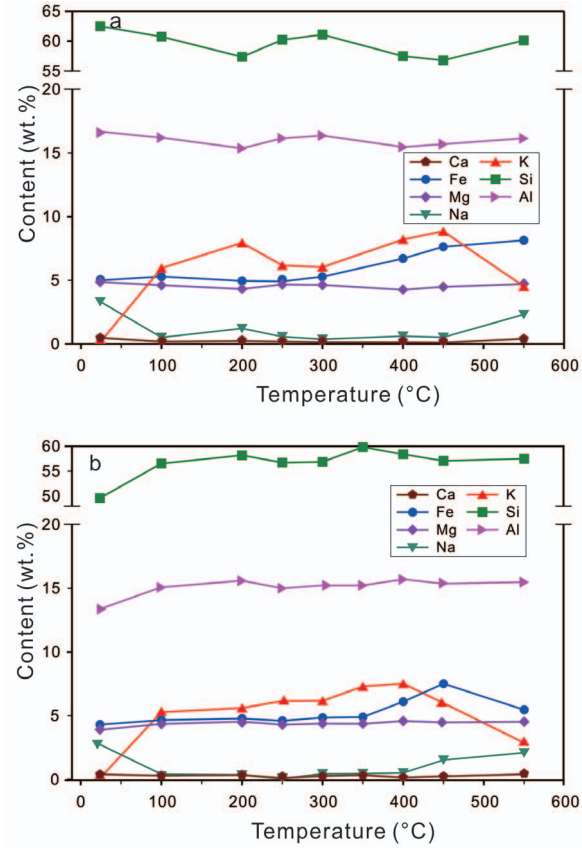

Figure 5. Variations in the Ca, Fe, Mg, Na, K, Si, and Al contents of (a) M1 and (b) M2 with temperature.

Near infrared (NIR) analysis. Spectroscopic analysis using NIR (1250−2500 nm) can identify the combined stretching and bending vibrations of H_2O bound to smectites at 1905 nm and the stretching vibrations of structural OH groups and H_2O molecules in smectites at 1400 nm (Figure 8). In the M1 samples, the intensities of the bands at 1905 and 1400 nm decreased with increased temperatures and the rate of decrease was faster when the temperature was >350ºC. In the M2 samples, the intensities of bands at 1905 and 1400 nm also decreased with increased temperatures, but the rate of decrease was lower than that in M1 when temperatures were >350ºC. These characteristics indicate subtle differences in the smectite structures of M1 and M2.

DISCUSSION

Smectite illitization characteristics

At a sample treatment temperature of 350ºC, marked changes in the characteristics, such as clay content, I-S stacking mode, %I in I-S, and N_{ave} (Figures 2 and 3) occurred. When the temperature of M1 was <350ºC, the illite content was higher than in M2 (Figures 2a, 2e) and the changes in N_{ave} and I-S stacking mode with increased temperature were faster in M1 than in M2.

https://doi.org/10.1346/CCMN.2017.064084 Published online by Cambridge University Press

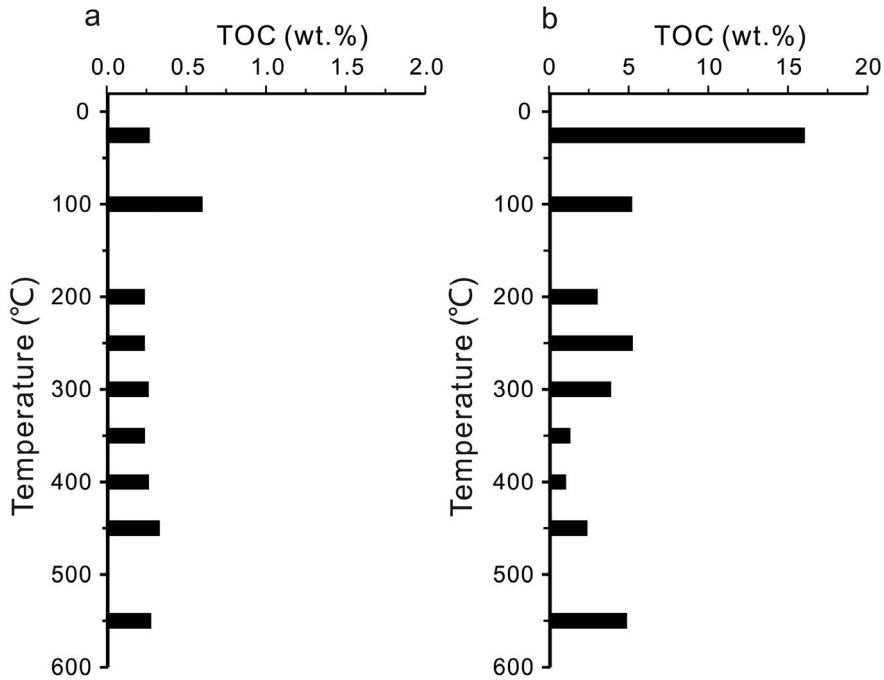

Figure 6. Variations in total organic carbon (TOC) contents of (a) M1 and (b) M2 with temperature. The TOC contents of M1 ranged from 0.23 to 0.6%, whereas the TOC contents of M2 ranged from 1.02 to 16.02%.

This suggests that the speed of smectite illitization was faster in M1 than in M2. When the temperature exceeded 350ºC, the illite and %I in I-S contents in M1 were lower than in M2 (Figures 2a, 2e). The change of N_{ave} in M1 was linear (Figure 2f) and the I-S stacking mode increased to R1.5 (Figure 3). This indicates that the degree of smectite illitization in M1 was higher than in M2 and that the speed of smectite illitization in M2 was faster than in M1. The reasons for changes in the speed and degree of smectite illitization at 350ºC is worthy of a focused investigation.

The bulk mineralogies of M1 and M2 were obviously changed with increased temperature. First, the relative contents of quartz, halite, K-feldspar, plagioclase, and ankerite in M1 and M2 increased with temperature (Table 1, Figure 1). The Si, Al, Ca, Mg, K, Na, and Fe contents changed with increased temperature (Table 1, Figure 5). Second, in the M1 samples heated at <300ºC,

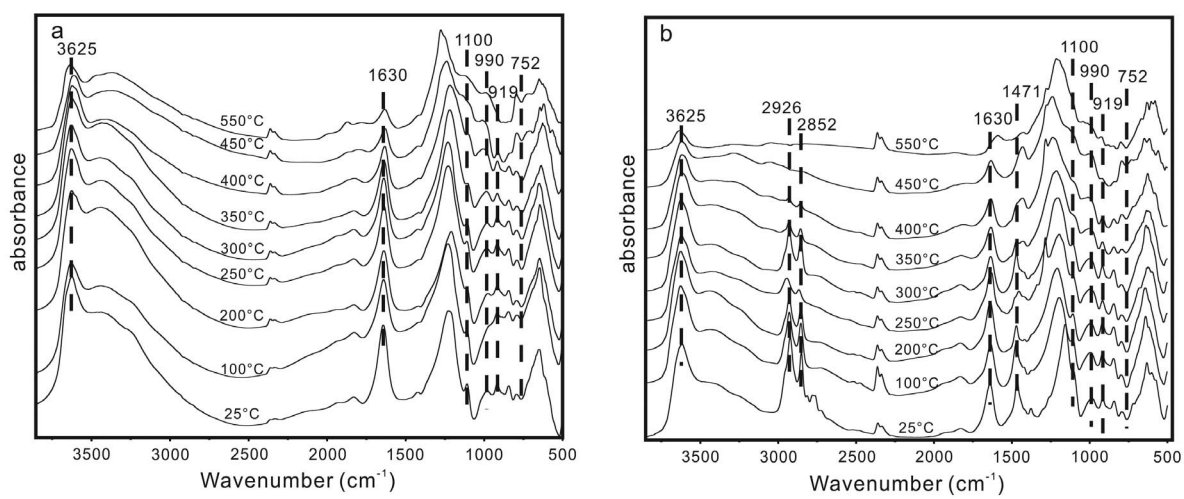

Figure 7. The FTIR spectra of (a) M1 and (b) M2 at different temperatures. The M1 and M2 samples had the OH stretching vibration (3625 cm^{-1}), the Si-O antisymmetric stretching vibrations (1100 and 990 cm^{-1}), and the Al-OH bending vibrations (919 and 752 cm^{-1}). The M2 sample had a distinct C-H vibrations (2926 and 2852cm^{-1}).

https://doi.org/10.1346/CCMN.2017.064084 Published online by Cambridge University Press

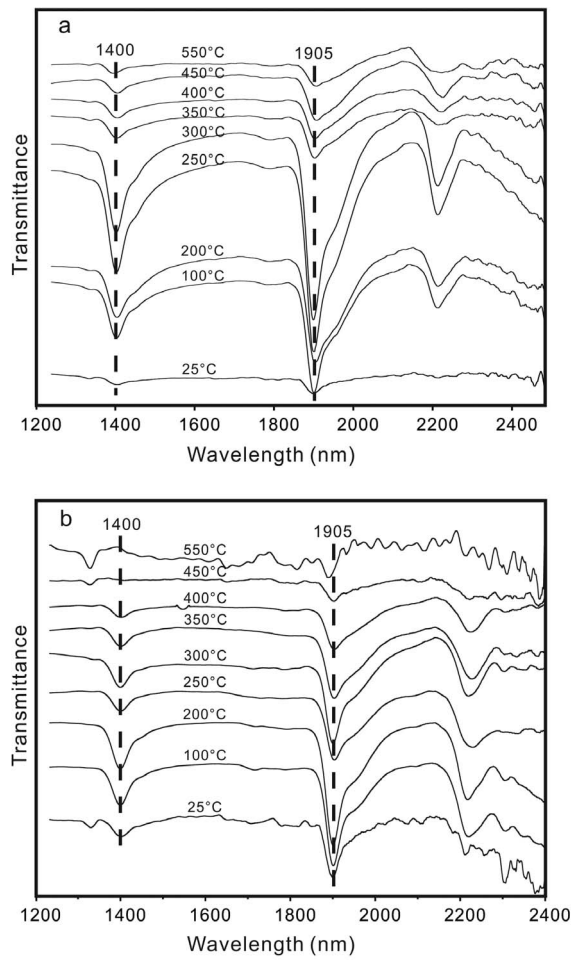

Figure 8. The NIR spectra of (a) M1 and (b) M2 at different temperatures. The band near 1905 nm is attributed to the first overtone of water molecules ($2\nu H_2O$) and first overtone of structural OH groups ($2\nu OH$). The band near 1400 nm was the combined stretching and bending vibrations of water ($\nu+\delta$) H_2O, where ν denotes the stretching vibration and δ denotes the bending vibration.

the clay mineral contents were relatively high; halite formed and the quartz, K-feldspar, and plagioclase contents increased relative to the unheated sample. The element contents were relatively stable except for the large changes in K and Na contents with temperature. In the M1 samples heated at >300ºC, the clay mineral content was relatively low; halite and ankerite formed and the relative contents of quartz, K-feldspar, and plagioclase increased; and the K, Na, and Fe contents greatly changed with temperature. In the M2 samples heated at <300ºC, the mineralogy and elemental contents were similar to that of the M1 samples heated at <300ºC, except no plagioclase was detected; in the M2 samples heated at >300ºC, the mineralogy and elemental contents were also the same as those in the M1 samples heated at >300ºC, a small amount of plagioclase was only evident in the sample heated at 350ºC, and ankerite was evident in samples heated at different temperatures. These characteristics clearly show variations in the bulk mineralogy of M1 and M2 with increased temperature.

OM characteristics and evolution

The essential difference between the M1 and M2 samples was that M1 is a pure smectite and has less TOC than M2 (Table 1, Figure 6). The XRD patterns of the heated $M1_{25ºC}$ sample had smectite d_{001} values that decreased to nearly 1.0 nm when heated to 250ºC and 550ºC (Figure 9a), which indicates that the smectite interlayers in $M1_{25ºC}$ contain water and cations, but little or no OM (Nemecz, 1981; Cai, 2004). The XRD patterns of heated $M2_{25ºC}$ samples, however, had smectite d_{001} values for air-dried samples that were similar to samples prepared at 250ºC and subsequently decreased to 1.0 nm at 550ºC (Figure 9b). This indicates that OM was in the $M2_{25ºC}$ smectite interlayers (Nemecz, 1981; Cai, 2004). The differences in the M1 and M2 OM contents were also evident in the FTIR spectra, where the CH_2 vibration bands at 2926 and 2852 cm^{-1} were absent in the M1 spectra, but were present in M2 spectra (Alstadt *et al.*, 2012; Li *et al.*, 2015; Li *et al.*, 2016). These characteristics revealed that the OM in M1 was only adsorbed to external surfaces and that the OM in M2 was mainly adsorbed into smectite interlayers.

The XRD patterns of heated M2 samples have d_{001} interlayer spacings in samples heated at <350ºC that are greater than 1 nm in both the air-dried and 250ºC heated samples. The M2 d_{001} value decreased to 1 nm after heating at 550ºC (Figure 9b), which suggests that the OM was in the M2 smectite interlayers (Theng *et al.*, 1986; Yariv and Lapides, 2005; Cai *et al.*, 2007). When the temperature exceeded 350ºC, the d_{001} interlayer spacing in the 250ºC treatment samples sharply decreased to 1 nm (Figure 9b), which suggests that most of the OM in the M2 smectite interlayers had been lost (Li *et al.*, 2016). The FTIR spectra of the M2 samples heated at <350ºC indicated no change in the CH_2 vibration bands at 2926 and 2852 cm^{-1} (Nguyen *et al.*, 1991; Ge *et al.*, 2009), but weakened and finally disappeared in M2 samples heated at >350ºC (Figure 7). This indicates that the OM adsorbed to smectite was released when the temperature reached 350ºC. Considering the changes in the XRD patterns and FTIR spectra of samples heated at increased temperatures, the 350ºC heating temperature demarcates the OM adsorption behavior of smectite, which is in agreement with the evolution of smectite illitization.

In addition, the desorption of OM adsorbed to minerals (Kennedy *et al.*, 2002; Ding and Shang, 2010) and hydrothermal experiments in hydrocarbon generation (Yang *et al.*, 2015) have revealed that OM adsorbed to smectite can be desorbed to release hydrocarbons and CO_2. When the temperature reaches 300 to 350ºC, the OM or hydrocarbons can be cracked to form light hydrocarbons or CO_2 (He *et al.*, 2013; Zheng *et al.*, 2014).

https://doi.org/10.1346/CCMN.2017.064084 Published online by Cambridge University Press

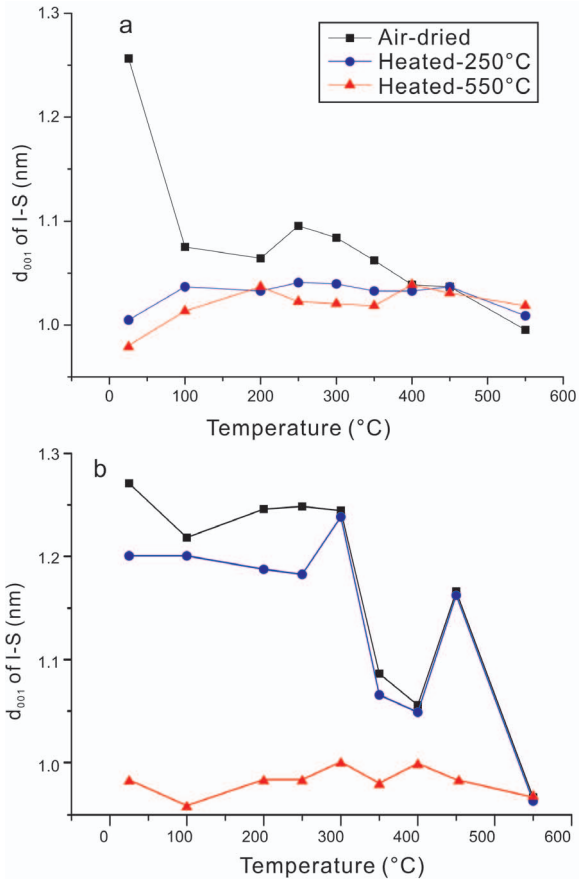

Figure 9. Variations in interlayer spacings of I-S in (a) M1 and (b) M2 under air-dried, heated to 250ºC, and heated to 550ºC treatments. The d_{001} peak was determined using the Jade® 6.5 computer software (Materials Data Inc., Livermore, California, USA) program.

Thus, hydrocarbons or CO_2 may have been released in this study when treatment temperatures exceeded 350ºC, which is crucial to understand the changes in mineral assemblages in hydrothermal experiments.

Influence of OM on smectite illitization

The differences between the interlayer materials in smectite and in illite determine that illitization must be accompanied by the exchange of interlayer cations (Altaner and Ylagan, 1997). The M1 and M2 hydrothermal experiments revealed that: a) the degree of M1 smectite illitization linearly increased with increased temperature, but smectite illitization increased *via* two stages in M2, although $M1_{25ºC}$ and $M2_{25ºC}$ had the same mineralogical characteristics and the degree of smectite illitization in M1 differed from M2; b) the $M1_{25ºC}$ and $M2_{25ºC}$ interlayers were initially Na-saturated and the interlayer spacing (d_{001} of I-S) and the Na^+ contents decreased with increased temperature, whereas the K^+ contents increased (Table 1, Figures 3 and 5) and suggests that interlayer cations were exchanged in the smectite; and c) the greatest difference between M1 and M2 was in the OM content (Table 1, Figure 6) where the M1 interlayers contained water and hydrated cations and the M2 interlayers mostly contained OM. The OM in M2 interlayers was largely released when the temperature exceeded 350ºC (Figures 4b and 9b). Thus, the differences in how smectite illitization evolved in M1 and M2 were mainly attributed to the interlayer OM. Previous studies have indicated that smectites can adsorb OM *via* ionic bonds, hydrogen bonds, and 'water bridges' in the interlayers (Theng, 1974; Lu *et al.*, 2011; Cai *et al.*, 2012). The stability of adsorbed OM can be enhanced (Theng *et al.*, 1986; Schulten *et al.*, 1996; Lu *et al.*, 1999; Yariv and Cross, 2002; Cai *et al.*, 2013) and the interlayer CEC suppressed (Pusino *et al.*, 1993). Cai *et al.* (2012) found that the OM adsorbed in clay mineral interlayers *via* 'water bridges' can delay the expulsion of interlayer water. The present study proposes that when smectite interlayers have only hydrated inorganic exchange ions (*e.g.*, M1), interlayer water is expelled and K^+ is exchanged as the temperature is increased, which gradually causes the transformation of smectite to illite (Table 1, Figure 10). When smectite interlayers contain OM (*e.g.*, M2), the exchange of K^+ for interlayer cations is slowed down because of the stability of interlayer OM. This stability decreases the speed of smectite to illite transformation. When temperatures exceed 350ºC, large amounts of interlayer OM are expelled, interlayer K^+ is increased, and smectite illitization is, thereby, accelerated to cause the two-stage smectite illitization process observed in M2 (Figure 10). The differences between M1 and M2 in the degree of smectite illitization, therefore, are ascribed to the inhibition caused by adsorbed OM (particularly, interlayer OM).

During the smectite illitization process, changes not only occur in interlayer water and smectite exchange cations, but also in the tetrahedral and octahedral sheets and in newly formed minerals (Peltonen *et al.*, 2009; Thyberg *et al.*, 2010; Metwally and Chesnokov, 2012). A comparison between M1 and M2 in the hydrothermal experiments revealed that: a) new minerals were formed and smectite illitization occurred as temperature was increased, and that 350ºC was a critical temperature for the formation of new minerals in both M1 and M2; b) the changes in Si and Al contents with increased temperature were subtle, but relative changes in the Na, K, and Fe contents were obvious and dramatically increased at >350ºC (Figure 10); and c) with increased temperature, the intensities of both the tetrahedral sheet Si-O antisymmetric stretching vibrations at 1100 and 990 cm^{-1} and the octahedral sheet Al-OH bending vibrations at 919 and 752 cm^{-1} were changed in M1 and M2. The intensity of the Si-O antisymmetric stretching vibration in the tetrahedral sheet was relatively stable when the temperatures were below 350ºC, but decreased when the temperature exceeded 350ºC (Figure 7). In smectite, the

https://doi.org/10.1346/CCMN.2017.064084 Published online by Cambridge University Press

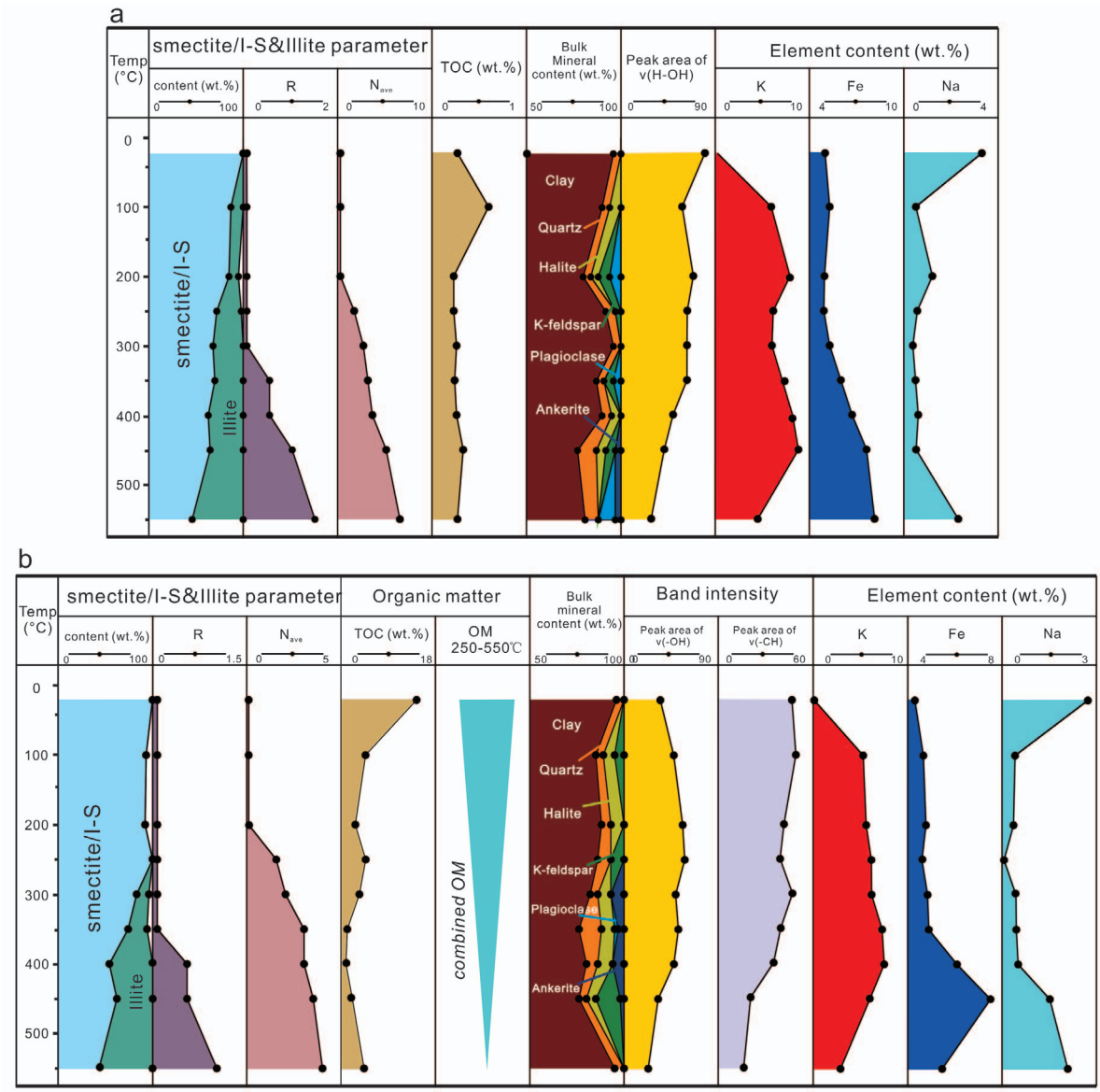

Figure 10. Variations in clay mineralogy, OM, bulk mineralogy, band intensity, and element content of (a) M1 and (b) M2 with temperature. The clay mineralogy data consists of mineral content, stacking mode of I-S (R), and average number of layers in I-S (N_{ave}). The band intensity is the peak area of νOH and νCH (ν denotes the stretching vibration). The K, Fe, and Na contents varied with temperature.

changes in the structural OH (1400 nm) and H_2O vibrations were similar to those in the tetrahedral sheet Si-O groups (Figure 8); d) ankerite appeared when the temperature exceeded 300ºC and was closely correlated with the changes in OM. Previous studies have indicated that Si and Al in the tetrahedral and octahedral sheets can be changed to form new minerals during smectite illitization (Peltonen *et al.*, 2009; Metwally and Chesnokov, 2012). The OM was cracked to form light hydrocarbons or CO_2 when the temperature reached 300 to 350ºC (He *et al.*, 2013; Zheng *et al.*, 2014). Based on the findings above, Si and Al ions can be released from smectite tetrahedral and octahedral sheets when the temperature exceeds 350ºC. When OM is present and the temperatures are >300ºC, OM can be cracked to form CO_2 (He *et al.*, 2013; Zheng *et al.*, 2014) and the Mg^{2+} and Ca^{2+} released during smectite illitization can provide the fundamental materials (*e.g.* Ca, Fe, Mg, Mn, and HCO_3) needed to form ankerite ($Ca(Fe, Mg, Mn)(CO_3)$).

Significance

Variations in M1 and M2 smectite illitization during hydrothermal experiments were due to different mineral evolutions in the M1 water-rock system and the M2

https://doi.org/10.1346/CCMN.2017.064084 Published online by Cambridge University Press

water-rock-OM system. Under the same conditions, smectite illitization was greater in the water-rock system than in the water-rock-OM system. This suggests that the smectite illitization in mudstones differs in water-rock and water-rock-OM systems (*i.e.*, without and with OM) of the same basin. A marked change occurred in smectite illitization at 350ºC in both the water-rock system (M1) and the water-rock-OM systems (M2). Smectite illitization is a linear process in the water-rock system and is a two-stage process in the water-rock-OM system (M2). This indicates a variation in the degree of smectite illitization in different systems due to the presence or absence of OM. Thus, special attention should be paid when using the crystallinity of I-S and illite to estimate geological temperature. As smectite illitization evolves in both water-rock and water-rock-OM systems, the tetrahedral and octahedral sheets are changed and exhibit the systematic characteristics of diagenesis. When the OM is cracked to produce CO_2 at temperature >300ºC, ankerite can be formed when smectite illitization occurs in the presence of OM. This study should inspire further investigations into the mechanisms of mineral formation, organic-mineral interactions, hydrocarbon formation, and the carbon cycle in water-rock-OM systems.

ACKNOWLEDGMENTS

This work was financially supported by the National Natural Science Foundation of China (Grant No. 41672115) and the National Oil and Gas Special Fund (Grant No.2016ZX05006e001-003).

REFERENCES

Ahn, J. and Peacor, D. (1986) Transmission and analytical electron microscopy of the smectite-to-illite transition. *Clays and Clay Minerals*, **34**, 165–179.

Alstadt, K.N., Katti, D.R., and Katti, K.S. (2012) An *in situ* FTIR step-scan photoacoustic investigation of kerogen and minerals in oil shale. *Spectrochimica Acta Part A: Molecular and Biomolecular Spectroscopy*, **89**, 105–113.

Altaner, S. and Ylagan, R. (1997) Comparison of structural models of mixed-layer illite/smectite and reaction mechanisms of smectite illitization. *Clays and Clay Minerals*, **45**, 517–533.

Armstrong, D.E. and Chesters, G. (1964) Properties of protein-bentonite complexes as influenced by equilibration conditions. *Soil Science*, **98**, 39–52.

Arnarson, T.S. and Keil, R.G. (2007) Changes in organic matter–mineral interactions for marine sediments with varying oxygen exposure times. *Geochimica et Cosmochimica Acta*, **71**, 3545–3556.

Balsam, W.L. and Deaton, B.C. (1991) Sediment dispersal in the Atlantic Ocean: Evaluation by visible light spectra. *Reviews in Aquatic Sciences*, **4**, 411–447.

Baronnet, A. (1997) Silicate microstructures at the sub-atomic scale. *Comptes Rendus de l'Académie des Sciences. Série 2. Sciences de la Terre et des Planètes (in French)*, **324**, 157–172.

Berthelin, J. (2010) Soil microorganism-mineral-organic matter interactions and the impact on metal mobility. Pp. 49–51 in: *Molecular Environmental Soil Science at the Interfaces in the Earth's Critical Zone* (J. Xu and P.M. Huang, editors). Springer, Hangzhou, China.

Bethke, C.M. and Altaner, S. (1986) Layer-by-layer mechanism of smectite illitization and application to a new rate law. *Clays and Clay Minerals*, **34**, 136–145.

Boles, J.R. and Franks, S.G. (1979) Clay diagenesis in Wilcox sandstones of southwest Texas: Implications of smectite diagenesis on sandstone cementation. *Journal of Sedimentary Research*, **49**, 55–70.

Burst, J.F. (1969) Diagenesis of Gulf Coast clayey sediments and its possible relation to petroleum migration. *AAPG Bulletin*, **53**, 73–93.

Cai, J. (2004) *Organic-complexes in Muddy Sediment and Mudstone*. Science Press, Beijing, China, 212 pp.

Cai, J., Bao, Y., Yang, S., Wang, X., Fan, D., Xu, J., and Wang, A. (2007) Research on preservation and enrichment mechanisms of organic matter in muddy sediment and mudstone. *Science China: Earth Science*, **50**, 765–775.

Cai, J., Lu, L., Bao, Y., Fan, F., and Xu, J. (2012) The significance and variation characteristics of interlayer water in smectite of hydrocarbon source rocks. *Science China: Earth Science*, **55**, 397–404.

Cai, J., Song, M., Lu, L., Bao, Y., Ding, F., and Xu, J. (2013) Organo-clay complexes in source rocksùa natural material for hydrocarbon generation. *Marine Geology and Quaternary Geology*, **33**, 123–131.

Cuadros, J. (2012) Clay crystal-chemical adaptability and transformation mechanisms. *Clay Minerals*, **47**, 147–164.

Cuadros, J. and Altaner, S.P. (1998) Compositional and structural features of the octahedral sheet in mixed-layer illite/smectite from bentonites. *European Journal of Mineralogy*, **10**, 111–124.

Cuadros, J. and Linares, J. (1996) Experimental kinetic study of the smectite-to-illite transformation. *Geochimica et Cosmochimica Acta*, **60**, 439–453.

Dickens, A.F., Baldock, J.A., Smernik, R.J., Wakeham, S.G., Arnarson, T.S., Gélinas, Y., and Hedges, J.I. (2006) Solid-state ^{13}C NMR analysis of size and density fractions of marine sediments: Insight into organic carbon sources and preservation mechanisms. *Geochimica et Cosmochimica Acta*, **70**, 666–686.

Ding, C. and Shang, C. (2010) Mechanisms controlling adsorption of natural organic matter on surfactant-modified iron oxide-coated sand. *Water Research*, **44**, 3651–3658.

Drits, V.A., Lindgreen, H., and Salyn, A.L. (1997) Determination of the content and distribution of fixed ammonium in illite-smectite by X-ray diffraction: Application to North Sea illite-smectite. *American Mineralogist*, **82**, 79–87.

Eberl, D. (1978) Reaction series for dioctahedral smectites. *Clays and Clay Minerals*, **26**, 327–340.

Eberl, D. and Srodon, J. (1988) Ostwald ripening and interparticle-diffraction effects for illite crystals. *American Mineralogist*, **73**, 1335–1345.

Egli, M., Mirabella, A., and Fitze, P. (2001) Clay mineral transformations in soils affected by fluorine and depletion of organic matter within a time span of 24 years. *Geoderma*, **103**, 307–334.

GBT 14506.28-2010, 2010. Methods for chemical analysis of silicate rocks-Part 28: Determination of 16 major and minor elements content. Standards Press of China, Beijing.

Ge, Y., Liu, L., and Ji, J. (2009) Rapid quantification of calcite in North Atlantic sediments by drifts and its climate significance-example of drilling site U1308. *Geological Journal of China Universities*, **15**, 184–191.

Greenwood, P., Brocks, J., Grice, K., Schwark, L., Jaraula, C., Dick, J., and Evans, K. (2013) Organic geochemistry and mineralogy. I. Characterisation of organic matter associated with metal deposits. *Ore Geology Reviews*, **50**, 1–27.

Grim, R.E. (1953) *Clay Mineralogy*. McGraw-Hill, New York, 596 pp.

Hanke, A., Sauerwein, M., Kaiser, K., and Kalbitz, K. (2014) Does anoxic processing of dissolved organic matter affect organic–mineral interactions in paddy soils? *Geoderma*, **228**, 62–66.

He, H., Frost, R.L., Bostrom, T., Yuan, P., Duong, L., Yang, D., Xi, Y., and Kloprogge, J.T. (2006) Changes in the morphology of organoclays with HDTMA+ surfactant loading. *Applied Clay Science*, **31**, 262–271.

He, H., Guo, J., Xie X., and Pen, J.(1999) Experimental studies on the selective adsorption of Cu^{2+}, Pb^{2+}, Zn^{2+}, Cd^{2+}, Cr^{2+} ions on montmorillonite, illite and kaolinite and the influence of medium conditions. *Acta Mineralogical Sinica*, **19**, 231–235.

He, K., Zhang, S., Wang, X., Mi, J., Mao, R., and Hu, G. (2013) Effect of gas generation from *in situ* cracking of residual bitumen in source on hydrocarbon generation from organic matter. *Acta Petrolei Sinica*, **34**, 57–64.

Howard, J.J. and Roy, D. (1985) Development of layer charge and kinetics of experimental smectite alteration. *Clays and Clay Minerals*, **33**, 81–88.

Hower, J., Eslinger, E.V., Hower, M.E., and Perry, E.A. (1976) Mechanism of burial metamorphism of argillaceous sediment: 1. Mineralogical and chemical evidence. *Geological Society of America Bulletin*, **87**, 725–737.

Huang, W.L., Longo, J.M., and Pevear, D.R. (1993) An experimentally derived kinetic model for smectite-to-illite conversion and its use as a geothermometer. *Clays and Clay Minerals*, **41**, 162–162.

Inoue, A., Kohyama, N., Kitagawa, R., and Watanabe, T. (1987) Chemical and morphological evidence for the conversion of smectite to illite. *Clays and Clay Minerals*, **35**, 111–120.

Inoue, A., Watanabe, T., Kohyama, N., and Brusewitz, A.M. (1990) Characterization of illitization of smectite in bentonite beds at Kinnekulle, Sweden. *Clays and Clay Minerals*, **38**, 241–249.

Kennedy, M.J., Pevear, D.R., and Hill, R.J. (2002) Mineral surface control of organic carbon in black shale. *Science*, **295**, 657–660.

Kothawala, D., Roehm, C., Blodau, C., and Moore, T. (2012) Selective adsorption of dissolved organic matter to mineral soils. *Geoderma*, **189**, 334–342.

Lanson, B., Sakharov, B.A., Claret, F., and Drits, V.A. (2009) Diagenetic smectite-to-illite transition in clay-rich sediments: A reappraisal of X-ray diffraction results using the multi-specimen method. *American Journal of Science*, **309**, 476–516.

Lasaga, A.C. and Luttge, A. (2001) Variation of crystal dissolution rate based on a dissolution stepwave model. *Science*, **291**, 2400–2404.

Leithold, E.L., Perkey, D.W., Blair, N.E., and Creamer, T.N. (2005) Sedimentation and carbon burial on the northern California continental shelf: The signatures of land-use change. *Continental Shelf Research*, **25**, 349–371.

Li, J. and David, J.B. (2005) Palynofacies: Principles and methods. *Acta Palaeontologica Sinica*, **44**, 138–156.

Li, Y., Cai, J., Song, G., and Ji, J. (2015) Drift spectroscopic study of diagenetic organic-clay interactions in argillaceous source rocks. *Spectrochimica Acta. Part A, Molecular and Biomolecular Spectroscopy*, **148**, 138–145.

Li, Y., Cai, J., Song, M., Ji, J., and Bao, Y. (2016) Influence of organic matter on smectite illitization: A comparison between red and dark mudstone from the Dongying Depression, China. *American Mineralogist*, **101**, 134–145.

Liu, W., Ni, Y., and Xiao, H. (2005) Preparation and characterization of hydrophobic cationic montmorillonite. *Transactions of China Pulp and Paper*, **20**, 169–173.

Lu, L., Cai, J., Liu, W., Teng, E., and Hu, W. (2011) Water bridges mechanism of organo smectite interaction in argillaceous hydrocarbon source rocks: Evidences from *in situ* drift spectroscopic study. *Oil & Gas Geology*, **32**, 47–55.

Lu, X., Hu, W., Fu, Q., Miao, D., Zhou, G., and Hong, Z. (1999) Study of combination pattern of soluble organic matters and clay minerals in the immature source rocks in Dongying Depression, China. *Scientia Geologica Sinica*, **34**, 72–80.

Mayer, L.M. (1994) Surface area control of organic carbon accumulation in continental shelf sediments. *Geochimica et Cosmochimica Acta*, **58**, 1271–1284.

Metwally, Y.M. and Chesnokov, E.M. (2012) Clay mineral transformation as a major source for authigenic quartz in thermo-mature gas shale. *Applied Clay Science*, **55**, 138–150.

Moore, D.M. and Reynolds, R.C. (1997). *X-ray Diffraction and the Identification and Analysis of Clay Minerals*. Oxford University Press, New York, 332 pp.

Mosser-Ruck, R., Cathelineau, M., Baronnet, A., and Trouiller, A. (1999) Hydrothermal reactivity of K-smectite at 300ºC and 100 bar: Dissolution-crystallization process and non-expandable dehydrated smectite formation. *Clay Minerals*, **34**, 275–290.

Mosser-Ruck, R., Pironon, J., Cathelineau, M., and Trouiller, A. (2001) Experimental illitization of smectite in K-rich solution. *European Journal of Mineralogy*, **13**, 829–840.

Nadeau, P., Wilson, M., McHardy, W., and Tait, J. (1985) The conversion of smectite to illite during diagenesis: Evidence from some illitic clays from bentonites and sandstones. *Mineralogical Magazine*, **49**, 393–400.

Naderizadeh, Z., Khademi, H., and Arocena, J. (2010) Organic matter induced mineralogical changes in clay-sized phlogopite and muscovite in alfalfa rhizosphere. *Geoderma*, **159**, 296–303.

Nemecz, E. (1981) *Clay Minerals*. Akademiai Kiado, Budapest, Hungary, 547 pp.

Nguyen, T., Janik, L.J., and Raupach, M. (1991) Diffuse reflectance infrared fourier transform (drift) spectroscopy in soil studies. *Soil Research*, **29**, 49–67.

Olives, J., Amouric, M., and Perbost, R. (2000) Mixed layering of illite-smectite: Results from high-resolution transmission electron microscopy and lattice-energy calculations. *Clays and Clay Minerals*, **48**, 282–289.

Pacton, M., Gorin, G.E., and Vasconcelos, C. (2011) Amorphous organic matter – experimental data on formation and the role of microbes. *Review of Palaeobotany and Palynology*, **166**, 253–267.

Parbhakar, A., Cuadros, J., Sephton, M.A., Dubbin, W., Coles, B.J., and Weiss, D. (2007) Adsorption of l-lysine on montmorillonite. *Colloids and Surfaces A: Physicochemical and Engineering Aspects*, **307**, 142–149.

Pearson, M. and Small, J. (1988) Illite-smectite diagenesis and palaeotemperatures in northern North Sea Quaternary to Mesozoic shale sequences. *Clay Minerals*, **23**, 109–132.

Peltonen, C., Marcussen, Ø., Bjørlykke, K., and Jahren, J. (2009) Clay mineral diagenesis and quartz cementation in mudstones: The effects of smectite to illite reaction on rock properties. *Marine and Petroleum Geology*, **26**, 887–898.

Pentrák, M., Bizovská, V. and Madejová, J. (2012) Near-IR study of water adsorption on acid-treated montmorillonite. *Vibrational Spectroscopy*, **63**: 360–366.

Pérez, M.A., Moreira-Turcq, P., Gallard, H., Allard, T., and Benedetti, M.F. (2011) Dissolved organic matter dynamic in the Amazon basin: Sorption by mineral surfaces. *Chemical Geology*, **286**, 158–168.

Perry, E.A. and Hower, J. (1970) Burial diagenesis in Gulf Coast pelitic sediments. *Clays and Clay Minerals*, **18**, 165–177.

Pollard, C.O. (1971) Appendix: Semidisplacive mechanism for

diagenetic alteration of montmorillonite layers to illite layers. *Geological Society of America Special Papers*, **134**, 79–94.

Pusino, A., Liu, W., and Gessa, C. (1993) Dimepiperate adsorption and hydrolysis on Al^{3+}, Fe^{3+}, Ca^{2+}, and Na^{+} montmorillonite. *Clays and Clay Minerals*, **41**, 335–340.

Putnis, A. (2002) Mineral replacement reactions: From macroscopic observations to microscopic mechanisms. *Mineralogical Magazine*, **66**, 689–708.

Ramseyer, K. and Boles, J. (1986) Mixed-layer illite/smectite minerals in Tertiary sandstones and shales, San Joaquin Basin, California. *Clays and Clay Minerals*, **34**, 115–124.

Reynolds, R.C. (1985). *NEWMOD, A Computer Program for the Calculation of One-dimensional Diffraction Patterns of Mixed-layered Clays*. Self-published, Hanover, New Hampshire.

Roberson, H.E. and Lahann, R.W. (1981) Smectite to illite conversion rates: Effects of solution chemistry. *Clays and Clay Minerals*, **29**, 129–135.

Schulten, H.R., Leinweber, P., and Theng, B. (1996) Characterization of organic matter in an interlayer clay-organic complex from soil by pyrolysis methylation-mass spectrometry. *Geoderma*, **69**, 105–118.

Środoń, J., Elsass, F., McHardy, W., and Morgan, D. (1992) Chemistry of illite-smectite inferred from TEM measurements of fundamental particles. *Clay Minerals*, **27**, 137–158.

Theng, B.K.G. (1974) *The Chemistry of Clay-organic Reactions*. Wiley, New York, USA, 343 pp.

Theng, B.K.G. (1979) *Formation and Properties of Clay-polymer Complexes*. Elsevier, Amsterdam, Netherlands, 362 pp.

Theng, B.K.G., Churchman, G., and Newman, R. (1986) The occurrence of interlayer clay-organic complexes in two New Zealand soils. *Soil Science*, **142**, 262–266.

Thyberg, B., Jahren, J., Winje, T., Bjørlykke, K., Faleide, J.I., and Marcussen, Ø. (2010) Quartz cementation in Late Cretaceous mudstones, northern North Sea: Changes in rock properties due to dissolution of smectite and precipitation of micro-quartz crystals. *Marine and Petroleum Geology*, **27**, 1752–1764.

Tissot, B. and Welte, D. (1984) *Petroleum Formation and Occurrence: A New Approach to Oil and Gas Exploration*. Springer, Berlin, Germany, 699 pp.

Tyson, R.V. (1993) Palynofacies analysis. Pp. 153–191 in: *Applied Micropalaeontology* (D.G. Jenkins, editor). Springer, Netherlands.

Velde, B. and Vasseur, G. (1992) Estimation of the diagenetic smectite to illite transformation in time-temperature space. *American Mineralogist*, **77**, 967–976.

Wang S. (1998) Stability of interlayer water of montmorillonite under burial conditions. *Bulletin of Mineralogy, Petrology and Geochemistry*, **17**, 211–216.

Whitney, G. (1990) Role of water in the smectite-to-illite reaction. *Clays and Clay Minerals*, **38**, 343–350.

Whitney, G. and Velde, B. (1993) Changes in particle morphology during illitization: An experimental study. *Clays and Clay Minerals*, **41**, 209–218.

Xu, S. and Harsh, J.B. (1992) Alkali cation selectivity and surface charge of 2:1 clay minerals. *Clays and Clay Minerals*, **40**, 567–567.

Yang, Y., Lei, T., Xing, L., Cai, J., Wu, Y., and Si, G. (2015) Oil generation abilities of chemically bound organic matter in different types of organic clay complexes. *Petroleum Geology & Experiment*, **37**, 487–493.

Yariv, S. and Cross, H. (2002) *Organo-clay Complexes and Interactions*. Dekker, New York, USA, 688 pp.

Yariv, S. and Lapides, I. (2005) The use of thermo-XRD-analysis in the study of organo-smectite complexes. *Journal of Thermal Analysis and Calorimetry*, **80**, 11–26.

Zheng, M., Li, J., Wu, X., Wang, M., Chen, X., and Wang, G. (2014) High-temperature pyrolysis gas-sourcing potential of organic matter in marine shale source rock system. *China Petroleum Exploration*, **19**, 1–11.

(*Received 1 August 2017; revised 30 January 2018; Ms. 1192; AE: J. Zhu*)